Aerotecnica Missili & Spazio, *The Journal of Aerospace Science, Technology and Systems*

Elastoplastic and progressive failure analysis of fiber-reinforced composites via an efficient nonlinear microscale model

I. Kaleel[a], M. Petrolo[b], E. Carrera[c]

[a] MUL^2 Group, Department of Mechanical and Aerospace Engineering, Politecnico di Torino, Italy

[b] MUL^2 Group, Department of Mechanical and Aerospace Engineering, Politecnico di Torino, Italy

[c] MUL^2 Group, Department of Mechanical and Aerospace Engineering, Politecnico di Torino, Italy

Abstract

This paper presents numerical results concerning the nonlinear and failure analysis of fiber-reinforced composites. The micromechanical framework exploits a class of refined 1D models based on the Carrera Unified Formulation (CUF) having a variable kinematic description. The recently developed CUF micromechanics is a framework for the nonlinear modeling and exploits the ability of the CUF to predict accurate 3D stress fields with reduced computational overheads. The present formulation features the von Mises J_2 theory for the pre-peak nonlinearity observed in matrix constituents, and the crack-band theory to capture the damage progression. Numerical examples and comparisons with results from literature assess the accuracy and efficiency of the proposed framework. The paper highlights the applicability of CUF models as an efficient micromechanical platform for nonlinear and progressive failure analysis for fiber-reinforced composites with potentially major advantages in the perspective of multiscale modeling.

1. Introduction

Recent advances in the field of high-performance computing have catalyzed the simulation-based design of materials and structural systems [1]. The usage of the virtual testing framework for composites has improved over the last couple of decades with significant advances in the field of multiscale methods [2]. Commercial packages such as DIGIMAT have also paved the way for efficient computation of virtual allowables and multiscale modeling for composite systems [3]. Accurate prediction of the nonlinear behavior of composites usually stretches the limits of these frameworks as users often come across accuracy versus analysis time trade-off. Scaling such frameworks for large-scale structural analyses remains an active field of research.

The nonlinear modeling of composites at ply-level often performs reasonably well for almost brittle failure. In the case of significant nonlinearities between first damage initiation and final failure, most of the standard ply-level damage criteria tend to be insufficient [4]. Methods based on multiscaling capabilities often perform better in such cases, but they come with a significant computational overhead. The high-fidelity generalized method of cells (HFGMC) micromechanics is one of the most recent advances to model nonlinear and progressive failure in composites [4, 5]. Zhang et al. [6] developed a multiscale computational model for deformation, damage, and failure response of hybrid 3D textile composite. The pre-peak nonlinear response stemmed from a modified J_2 deformation theory and the smeared crack approach modeled the post-peak softening. Chamis et al. developed a micromechanics-based progressive failure analysis framework for composites integrated with commercial FE packages [7]. Such a model can effectively capture different damage mechanisms. Davidson and Waas presented a novel approach to analyze the kink banding failure in composites through a microscale fiber-matrix unit cell modeling technique [8]. Another recent class of modeling approaches makes use of asymptotic analysis and the theory of structure genome [9].

The present work presents a nonlinear framework based on refined structural models to undertake the failure and nonlinear shear response of laminated composite structures. Built within the context of finite elements, refined models use the Carrera Unified Formulation (CUF) via a variable kinematic description [10]. Recently, CUF models successfully tackled a plethora of structural problems such as bio-mechanical structures [11], progressive failure analysis of composites [12], hygrothermal analysis of shells [13], buckling and post-buckling analyses of composite structures [14], and composite curved beam structures [15].

In this paper, the nonlinear behavior of composites at the microscale exploits the recently developed micromechanical framework based on CUF [16]. The micromechanics framework adopts the Component-Wise (CW) approach to model various components of the RVE through 1D finite element models. CUF-micromechanics models can effectively capture the nonlinear behavior with great computational efficiency [12, 16]. The present work uses two classes of constitutive material models; the von Mises based plasticity model [17] for the nonlinear shear response exhibited by the matrix and the crack-band model for the progressive failure analysis within the matrix [18].

The paper is organized as follows: Section 2 introduces CUF models, the finite element framework and the micromechanics modeling. Section 3 introduces the two classes of material models utilized to model the nonlinearity. Section 4 presents the numerical results and conclusions are in Section 5.

2. CUF micromechanics model

One-dimensional CUF models describe the kinematics of the structure through cross-section expansion functions, $F_\tau(x,z)$ and axial displacement functions $\mathbf{u}_\tau(y)$,

$$\mathbf{u} = \mathbf{u}_\tau(y)F_\tau(x,z), \quad \tau = 1, ..., M \tag{1}$$

where $\mathbf{u}$ is the generalized displacement vector, and M is the number of terms in the cross-section expansion function. The choice of F_τ and M remains arbitrary, and F_τ exploits various classes of basis functions, e.g., polynomial, harmonic or exponential. Three main classes of expansion functions emerged, namely, (a) Taylor-based expansion (TE) [19], (b) Lagrange-based expansion (LE) [20], and (c) Hierarchical Legendre-based expansions [21] (HLE). This work adopts LE. The micromechanical framework utilized in this work exploits the Component-Wise approach (CW), an extension of one-dimensional CUF models for complex structures such as RVE [16]. Using the CW approach, nine-node (L9) LE models interpolate the kinematic field over the cross-section. More details regarding LE are in [20].

2.1. Finite element approximation

The displacement vector is

$$\mathbf{u}(x,y,z) = \{u_x \quad u_y \quad u_z\}^T \tag{2}$$

The strain, ϵ, and stress, σ, vectors are

$$\boldsymbol{\epsilon} = \{\epsilon_{xx}\ \epsilon_{yy}\ \epsilon_{zz}\ \epsilon_{xy}\ \epsilon_{xz}\ \epsilon_{yz}\}^T, \tag{3}$$

$$\boldsymbol{\sigma} = \{\sigma_{xx}\ \sigma_{yy}\ \sigma_{zz}\ \sigma_{xy}\ \sigma_{xz}\ \sigma_{yz}\}^T \tag{4}$$

With small strain assumptions, the linear strain-displacement relations are

$$\boldsymbol{\epsilon} = \mathbf{D}\mathbf{u} \tag{5}$$

where $\mathbf{D}$ is the linear differential operator on $\mathbf{u}$. Section 3 provides the stress-strain relationship for different classes of nonlinear materials.

The finite element approximation exploits the shape functions $N_i(y)$ as follows:

$$\begin{aligned}\mathbf{u}(x,y,z) &= F_\tau(x,z)\ N_i(y)\ \mathbf{u}_{\tau i} \\ &\tau = 1, ..., M; \quad i = 1, ..., N_n\end{aligned} \tag{6}$$

where N_n is the number of nodes in the given finite element. Using the Principal of Virtual Displacement (PVD), the governing equations are

$$\delta L_{int} - \delta L_{ext} = 0 \tag{7}$$

where L_{int} stands for internal strain energy and L_{ext} for the work done by the external loads. The internal work is

$$\begin{aligned}\delta L_{int} &= \int_l \int_\Omega \delta\boldsymbol{\epsilon}^T \boldsymbol{\sigma}\, dx\, dz\, dy \\ &= \delta\mathbf{u}_{sj}^T\, \mathbf{k}_{ij\tau s}\, \mathbf{u}_{\tau i}\end{aligned}$$

where l and Ω are the axial and cross-section domains. $\mathbf{k}_{ij\tau s}$ is the fundamental nucleus if the stiffness matrix. The nucleus is a 3×3 and does not depend upon the order and type of expansion functions. A Newton-Raphson iteration scheme solves the system of nonlinear algebraic equations [22].

2.2. Component-wise micromechanics framework

Within the Component-Wise micromechanical framework, an RVE model has a beam FE along one axis, and the cross-section domain has 2D Lagrange elements, see Fig. 1. In other words, the FE acts along one axis. Otherwise, refined theories of structures act along the cross-section. Multiple LE elements discretize the cross-section of the RVE, enabling displacement and traction continuity across the interfaces of the various constituents. The beam has four-node (B4) elements. The present formulation uses periodic boundary conditions (PBC) consistently with the periodic assumptions of the RVE. More details concerning the numerical implementation of the Component-wise micromechanics framework are in [16].

3. Constitutive modeling

This paper uses two classes of material models for modeling nonlinearity in composites. The nonlinear shear response exhibited by unidirectional laminates has inelastic deformations within the matrix constituents. Plasticity-based inelastic models can simulate the shear-driven nonlinear behavior of matrix [23–25]. Based on the works of Bazant and Oh [18], the progressive failure analysis of matrix constituents under tension uses the crack-band model.

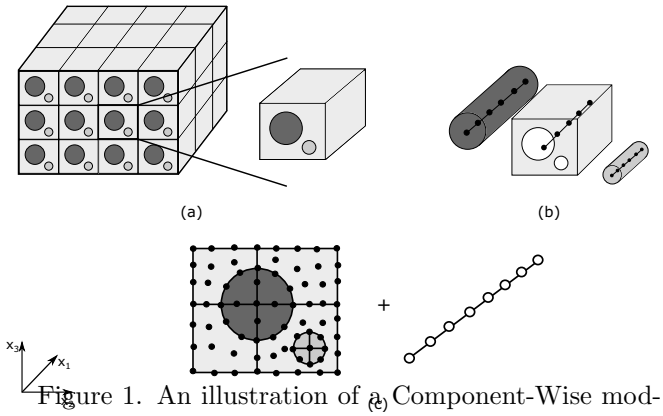

Figure 1. An illustration of a Component-Wise modeling of composite microstructure with arbitrary constituents: (a) a triply periodic composite microstructure with three different phases, (b) a triply periodic RVE with individual components modeled as separate components and (c) assembled cross-section with Lagrange elements along with the beam for the RVE [16].

3.1. Plasticity modeling

The constitutive relation for elastic constituents is

$$\boldsymbol{\sigma} = \boldsymbol{C}^e : \boldsymbol{\epsilon}^e \tag{8}$$

where $\boldsymbol{C}^e$ is the fourth-order elastic material matrix for individual constituents of composite, $\boldsymbol{\epsilon}^e$ is the elastic strain tensor, and $\boldsymbol{\sigma}$ is the stress tensor. Matrix has an elastoplastic constitutive model based on the von Mises J_2 theory [17]. The yield function ϕ is

$$\phi = \sigma_{eq} - R(\bar{\epsilon}_p) \tag{9}$$

where σ_{eq} is the equivalent von Mises stress, ϵ_p is the accumulated plastic strain and $R(\bar{\epsilon}_p)$ is the hardening function. Based on isotropic hardening assumption, the power law hardening function is [25]

$$R(\bar{\epsilon}_p) = R_0 + R_\infty(1 - \eta e^{\beta\epsilon_p})(1 - \eta e^{\mu\epsilon_p}) \tag{10}$$

where R_0 is the initial threshold, β, η and μ are parameters fitting the hardening curve. The flow rule determines the incremental plastic strain $d\epsilon_p$,

$$d\epsilon_p = d\lambda \frac{d\phi}{d\sigma} \tag{11}$$

where $d\lambda$ is the plastic multiplier and $d\phi/d\sigma$ provides the direction of the plastic flow. A return mapping numerical scheme using Newton-Raphson algorithm solves the local nonlinear problem. Numerical aspects of the implementation of plasticity model within CUF framework are in [22].

3.2. Crack-band model

The crack-band formulation models the progressive failure in matrix to capture the behavior of numerous microcracks formed in a given region and smear the effect over a finite volume [5, 18]. The maximum principal stress state determines the initiation and orientation of the crack-band in the matrix. The fracture toughness $\mathsf{G_c}$ of the matrix governs the traction-separation law and crack-band growth. In this work, crack propagation in the matrix is the mode I loading only. The local principal stress state $[\sigma_1^m, \sigma_2^m, \sigma_2^m]$ and principal directions $[\mathbf{n}_1^m, \mathbf{n}_2^m, \mathbf{n}_3^m]$ are computed at every integration point of matrix within the RVE. The crack-band initiates when the maximum principal stress (tensile) σ_1^m reaches the cohesive strength of the matrix σ_c^m,

$$\frac{\sigma_1^m}{\sigma_c^m} = 1 \tag{12}$$

Once initiated, the orientation of the crack-band remains fixed and the post-peak softening slope E_{IT} and the strain at failure ϵ_f become

$$\epsilon_f = \frac{2\mathsf{G_c}}{\sigma_c^m \mathsf{l_c}} \tag{13}$$

$$\mathsf{E}_{IT} = \left(\frac{1}{E_m^0} - \frac{\epsilon_f}{\sigma_c^m}\right)^{-1} \tag{14}$$

where $\mathsf{l_c}$ is the characteristic length of finite element and E_m^0 is the elastic Young modulus of the matrix. Further information on the crack-band model implementation within CUF is in [12].

4. Numerical Results

4.1. Nonlinear shear behavior of unidirectional composites

This section deals with the in-plane shear response of three different material systems via the CUF-micro framework; namely, (a) E-Glass-MY750, (b) HTA-6376, and (c) IM7-8552. Tables 1 and 2 enlist the calibrated material properties for the fiber and matrix constituents, respectively. The modeling of RVE the cross-section consists of 20 L9 elements, whereas along the third axis, the model has 2 B4 elements, see Fig. 2. The dimensions of the RVE are $10\,\mu m \times 10\,\mu m \times 0.1\,\mu m$ (length × width × thickness).

Table 3 shows the elastic properties of the material systems via the micromechanical framework. The hardening curve for the plasticity model exploits a four parameter model (see Eq. 10). The parameters fit the experimental nonlinear shear response. Table 4 enlists the calibrated hardening parameters for various matrix constituents and Fig. 3 depicts the hardening curve, whereas Fig. 4 shows the in-plane shear response for various material systems and comparisons with numerical and experimental results from the literature.

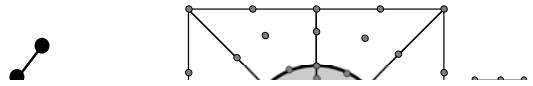

Figure 2. CW discretization of the square-packed RVE for the in-plane shear response of various unidirectional material systems

Table 1
Mechanical properties of fibers

Fiber type	E-Glass [26]	HTA [27]	IM7 [28]
$E_1{}^f$ (GPa)	74.0	223.0	272.5*
$E_2{}^f$ (GPa)	74.0	23.0	15.5*
$G_{12}{}^f$ (GPa)	30.8	32.0	29.0*
$G_{23}{}^f$ (GPa)	30.8	7.0	7.0
$\nu_{12}{}^f$ (-)	0.20	0.28	0.2

* Calibrated value

Table 2
Mechanical properties of matrix

Matrix type	MY750 [26]	6376C [27]	8552 [28]
E^m (GPa)	4.3*	3.7	4.1
G^m (GPa)	1.7	1.5	1.6
ν^m (-)	0.27*	0.20	0.29*

* Calibrated value

Table 3
Predicted elastic properties for three unidirectional laminates

Fiber Type	E-Glass	HTA	IM7
Matrix Type	MY750	6376	8552
V_f (%)	60	62	60
E_1 (GPa)	46.1	139.6	165.0
E_2 (GPa)	15.9	10.1	9.0
G_{12} (GPa)	5.9	5.9	5.6
G_{23} (GPa)	4.3	3.1	3.1
ν_{12} (-)	0.2	0.19	0.34

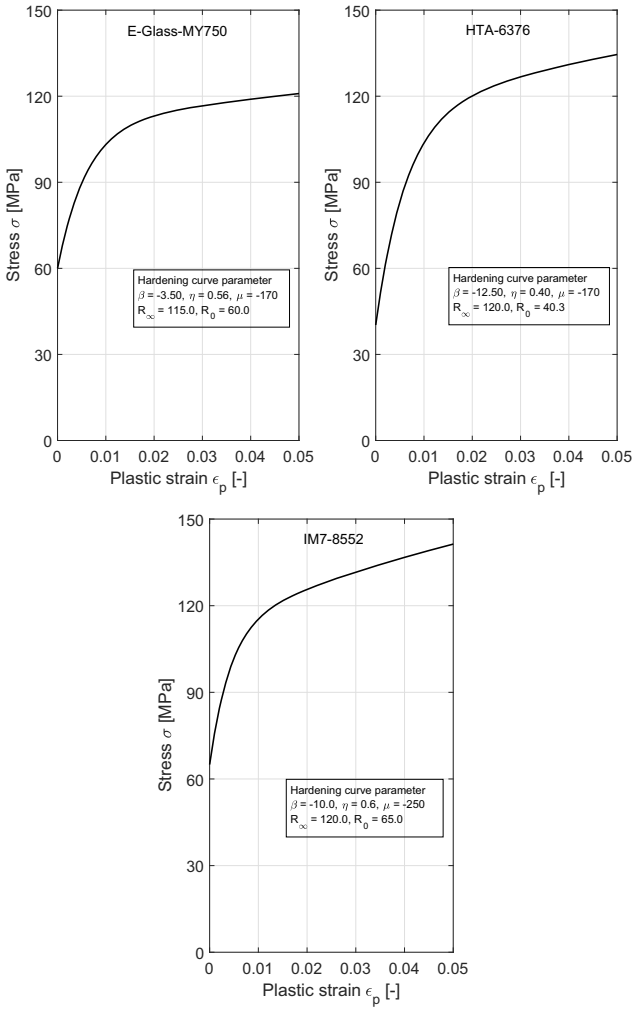

Figure 3. Hardening curve for three laminate systems with curve parameters

Table 4
Matrix hardening curve parameters

Matrix	R_0 (MPa)	R_∞ (MPa)	β (-)	η (-)	μ (-)
MY750	60.0	115.0	-3.5	0.56	-170.0
6376	40.3	120.0	-12.5	0.40	-170.0
8552	65.0	120.0	-10.0	0.60	-250.0

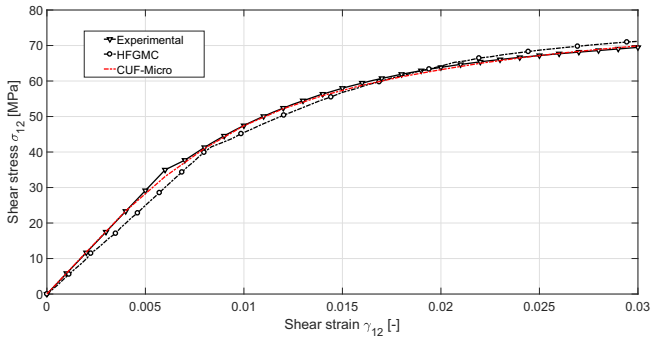

(a) E-Glass/MY750 (Experimental [26] and HFGMC [4])

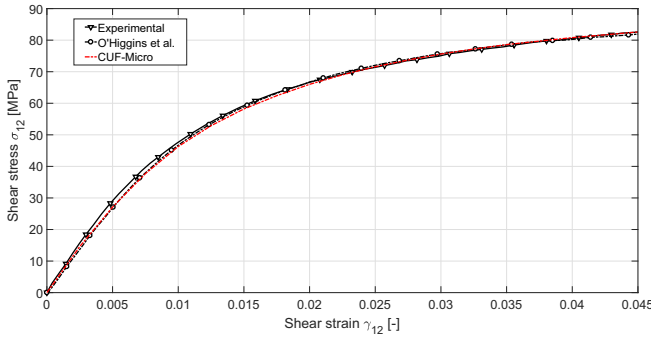

(b) HTA-6376 (Experimenal [29] and Higgins et al. [27])

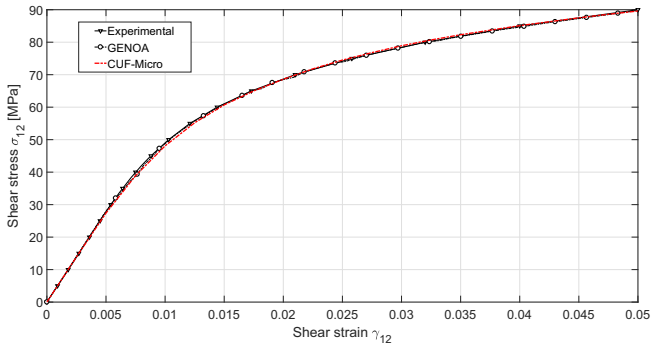

(c) IM7-8552 (Experimental [28] and GENOA [7])

Figure 4. Comparison of in-plane shear responses for various unidirectional material systems

The last numerical assessment of this section deals with a comparison between the standard finite element approach and CUF-micro models for predicting the shear response of the HTA-6376 material system. The study-case uses a square-packed RVE model having 1656 standard 3D brick elements, amounting to 6405 degrees of freedom. The mesh density of the 3D FEM model stemmed from a convergence study concerning the elastic stress field. As per the CUF-micro, the 3D model has periodic boundary conditions.

Figure 5 shows the in-plane shear response of HTA-6376 via the two methodologies. Table 5 lists the numerical results including the model information and analysis time.

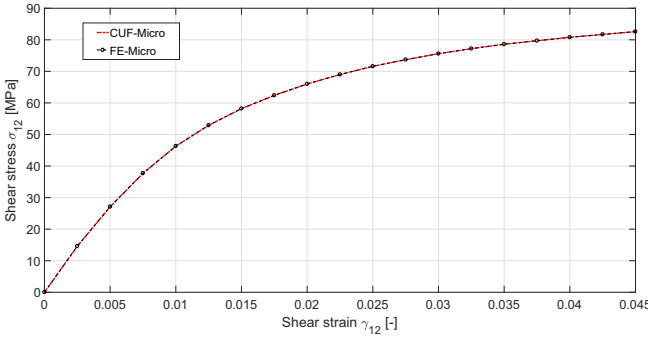

Figure 5. Comparison between 3D FEM and CUF-micro for the in-plane shear response of HTA-6376 material system

Table 5
Numerical results for from 3D FEM and CUF-micro model for the in-plane shear response of HTA-6376

	DOF	Number of Gauss points	Total analysis time [s]
CUF-micro	1,869	1,440	130
FE-micro	6,405	13,248	271

The results suggest that

1. CUF-micro models can accurately capture the nonlinear shear behavior with a good match with experimental and numerical results from the literature.

2. If compared to 3D FEM, CUF-micro models can capture the nonlinear behavior with high accu-

racy and lead to a reduction in the analysis time greater than 50%.

3. In CUF-micro models, the number of Gauss points required to store the state variables in the RVE is 9 times smaller than 3D FEM. Such a feature could significantly enhance the memory efficiency of a multiscale framework.

4.2. Progressive failure of a unidirectional fiber-reinforced composite under transverse tension

This section presents the progressive failure analysis of a uni-directional E-Glass/MY750 Epoxy composite under transverse tension. The objective is to capture the brittle post-peak softening behavior due to transverse cracking as evidenced experimentally [30]. In particular, this example extends the finding of CUF-micro from [12].

The numerical assessment considers a single fiber square-packed RVE architecture with 20 L9 and 2 B4 elements, and amounting to 1869 degrees of freedom, see Fig. 2.

The volume fraction of the RVE is 58% with dimensions of $8\,\mu m \times 8\,\mu m \times 0.8\,\mu m$. Tables 1 and 2 enlist the elastic properties for Silenka E-Glass and MY750 matrix, respectively. The calibrated tensile fracture properties for matrix, σ_c and G_c, are 66.5 MPa and 0.000563 N/mm, respectively [5, 31]. The fiber model is linear elastic. A global strain of 0.01 acts along the transverse direction (x_2) of the RVE.

Figure 6 shows the global transverse stress (σ_{22}) versus transverse strain (ϵ_{22}) along with comparisons against literature results based on GMC, HFGMC and standard 2D FE [31]. Table 6 enlists the numerical results along with the ultimate transverse stress and strain. Figure 7 shows the final damage contour at failure, whereas Fig. 8 shows the contour plots for the damage progression at the strain instances corresponding to the load drops.

The results suggest that

1. The ultimate transverse stress computed via CUF-micro has a good match with GMC, HFGMC, and FE-2D.

2. CUF-micro models produce similar damage progressions as observed in results from literature.

3. CUF-micro models can predict the step-wise load carrying capacity evidenced by experimental studies [30].

4. Figure 6 presents a step-wise behavior in the non-linear region. Such a behavior is due to the brittle nature of the failure leading to a step-wise reduction of the stiffness through the RVE in which the progression of damage proceeds as in Fig. 8.

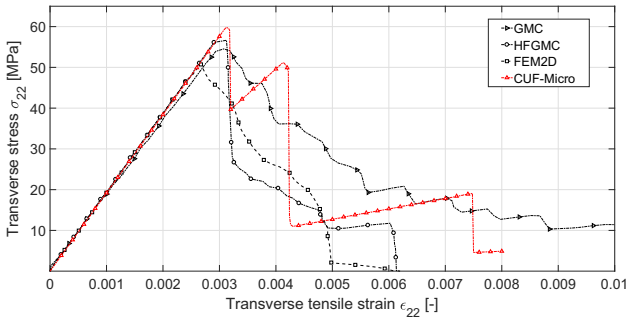

Figure 6. Transverse tensile stress versus strain curves of E-Glass/My750

Table 6
Numerical results for E-Glass/My750 under transverse strain

	Ultimate transverse stress [MPa]	Strain at ultimate transverse stress
GMC [31]	54.6	0.00310
HFGMC [31]	56.8	0.00313
FE-2D [31]	51.3	0.00267
CUF-micro	59.7	0.00314

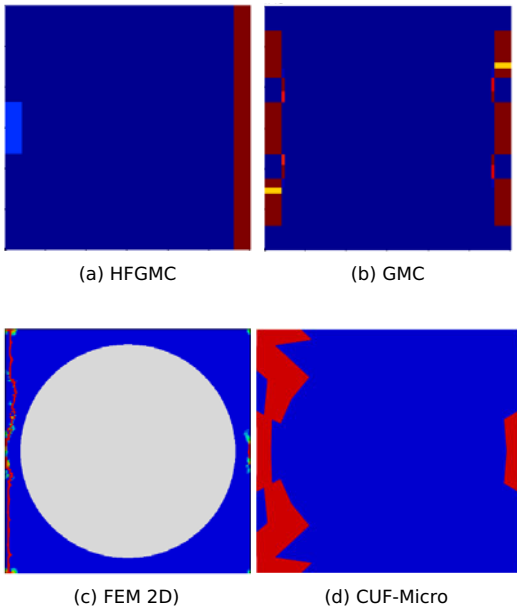

Figure 7. Final damage contour plots from CUF-micro and solutions from literature [31] of E-Glass/My750

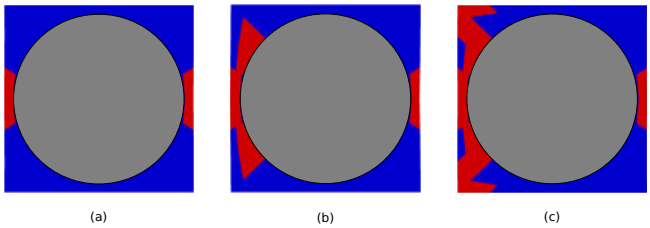

Figure 8. Damage progression for E-Glass/My750 under transverse strain at global strains (a) 0.0032, (b) 0.0054 and (c) 0.008

5. Conclusion

This paper presented numerical results concerning the nonlinear and progressive failure analysis of fiber-reinforced composites via the novel CUF micromechanical framework. The CUF modeling approach can handle each micro-component of a composite system with 1D structural models provide 3D-like stress fields. First, the numerical assessments considered the pre-peak nonlinearity exhibited by matrix constituents for three classes of fiber-reinforced composite materials. The results proved that CUF-micro can capture the nonlinear behavior with high accuracy if compared to experimental data. Furthermore, a comparison with the 3D FEM highlighted the numerical efficiency of CUF-micro, leading to a 50% reduction of the computational costs. The second study-case focused on the progressive failure via the crack-band model implemented within the CUF micromechanics. Predicted failure corresponds well with the reference results available from the literature and, in particular, the present model can detect the step-wise load drop evidenced by experimental campaigns.
Future work includes integrating the micromechanics toolbox within a multiscale framework to simulate large-scale composite structures.

6. Acknowledgement

This research work has been carried out within the project FULLCOMP (FULLy analysis, design, manufacturing, and health monitoring of COMPosite structures), funded by the European Union Horizon 2020 Research and Innovation program under the Marie Skłodowska-Curie grant agreement No. 642121.

REFERENCES

1. X. Liu, D. Furrer, J. Kosters, and J. Holmes. Vision 2040: A roadmap for integrated, multiscale modeling and simulation of materials and systems. NASA Glenn Research Center, 2018.
2. J. Llorca, C. González, J. M. Molina-Aldareguía, J. Segurado, R. Seltzer, F. Sket, M. Rodríguez, S. Sádaba, R. Muñoz, and L. P. Canal. Multiscale modeling of composite materials: A roadmap towards virtual testing. *Advanced Materials*, 23(44):5130–5147, 2011.
3. DIGIMAT Software. e-Xstream Engineering. Louvain-la-Neuve, Belgium, 2018.
4. B. A. Bednarcyk, J. Aboudi, and S. M. Arnold. Micromechanics Modeling of Composites Subjected to Multiaxial Progressive Damage in the Constituents. *AIAA Journal*, 48(7):1367–1378, 2010.
5. E. J. Pineda, B. A. Bednarcyk, A. M. Waas, and S. M. Arnold. Progressive failure of a unidirectional fiber-reinforced composite using the method of cells: Discretization objective computational results. *International Journal of Solids and Structures*, 50(9):1203–1216, 2013.
6. D. Zhang, A.M. Waas, and C.F. Yen. Progressive damage and failure response of hybrid 3D textile composites subjected to flexural loading, part II: Mechanics based multiscale computational modeling of progressive damage and failure. *International Journal of Solids and Structures*, 75-76:321–335, 2015.
7. C. C. Chamis, F. Abdi, M. Garg, L. Minnetyan, H. Baid, D. Huang, J. Housner, and F. Talagani. Micromechanics-based progressive failure analysis prediction for WWFE-III composite coupon test cases. *Journal of Composite Materials*, 47(20-21):2695–2712, 2013.
8. P. Davidson and A.M. Waas. Mechanics of kinking in fiber-reinforced composites under compressive loading. *Mathematics and Mechanics of Solids*, 21(6):667–684, 2016.
9. W. Yu. A unified theory for constitutive modeling of composites. *Journal of Mechanics of Materials and Structures*, 11(4):379–411, 2016.
10. E. Carrera, M. Cinefra, E. Zappino, and M. Petrolo. *Finite Element Analysis of Structures Through Unified Formulation*. 2014.
11. E. Carrera, D. Guarnera, and A. Pagani. Static and free-vibration analyses of dental prosthesis and atherosclerotic human artery by refined finite element models. *Biomechanics and Modeling in Mechanobiology*, 17(2):301–317, Apr 2018.
12. I Kaleel, M Petrolo, A M Waas, and E Carrera. Micromechanical Progressive Failure Analysis of Fiber- Reinforced Composite Using Refined Beam Models. *Journal of Applied Mechanics*, 85(February), 2018.
13. M. Cinefra, M. Petrolo, G. Li, and E. Carrera. Variable kinematic shell elements for composite laminates accounting for hygrothermal effects. *Journal of Thermal Stresses*, 40(12):1523–1544, 2017.
14. A. Pagani and E. Carrera. Large-deflection and

post-buckling analyses of laminated composite beams by Carrera Unified Formulation. *Composite Structures*, 170:40–52, 2017.

15. A.G. de Miguel, G. De Pietro, E. Carrera, G. Giunta, and A. Pagani. Locking-free curved elements with refined kinematics for the analysis of composite structures. *Computer Methods in Applied Mechanics and Engineering*, 337:481 – 500, 2018.
16. I. Kaleel, M. Petrolo, A.M. Waas, and E. Carrera. Computationally efficient, high-fidelity micromechanics framework using refined 1d models. *Composite Structures*, 181, 2017.
17. von Mises R. Mechanics of solid bodies in the plastically-deformable state. *Mechanik der festen Körper in plastisch-deformablen Zustand*, 4:582–592, 1913.
18. Z. Bazant and B. H. Oh. Crack band theory of concrete. *Materials and Structures*, 16:155–177, 1983.
19. E. Carrera and G. Giunta. Refined Beam Theories Based on a Unified Formulation. *International Journal of Applied Mechanics*, 02(01):117–143, 2010.
20. E. Carrera and M. Petrolo. Refined beam elements with only displacement variables and plate/shell capabilities. *Meccanica*, 47(3):537–556, 2012.
21. A Pagani, A. G. De Miguel, M. Petrolo, and E. Carrera. Analysis of laminated beams via Unified Formulation and Legendre polynomial expansions. *Composite Structure*, 156(15), 2016.
22. E. Carrera, I. Kaleel, and M. Petrolo. Elastoplastic analysis of compact and thin-walled structures using classical and refined beam finite element models. *Mechanics of Advanced Materials and Structures*, In Press.
23. C.T. Sun and Yoon K.J. Elastic-plastic analysis of as4/peek composite laminate using a one-parameter plasticity model. *Journal of Composite Materials*, 26(2):293–308, 1992.
24. M. Vogler, R. Rolfes, and P. P. Camanho. Mechanics of Materials Modeling the inelastic deformation and fracture of polymer composites -Part I : Plasticity model. *Mechanics of Materials*, 59:50–64, 2013.
25. Y. Zhou, C. Hou, W. Wang, M. Zhao, and X. Wan. A phenomenological intra-laminar plasticity model for frp composite materials. *IOP Conference Series: Materials Science and Engineering*, 87(1), 2015.
26. P D Soden, M J Hinton, and a S Kaddour. Biaxial test results for strength and deformation of a range of E-glass and carbon fibre reinforced composite laminates: Failure exercise benchmark data. *Composites Science and Technology*, 62:52–96, 2002.
27. O' Higgins R. M. *An experimental and numerical study of damage initiation and growth in high strength glass and carbon fiber-reinforced composite materials*. PhD thesis, University of Limerick, 2007.
28. A. Kaddour, M. Hinton, P. Smith, and S. Li. A comparison between the predictive capability of matrix cracking, damage and failure criteria for fibre reinforced composite laminates: Part A of the third world-wide failure exercise. *Journal of Composite Materials*, 47(20-21):2749–2779, 2013.
29. C. T. McCarthy, R. M. O'Higgins, and R. M. Frizzell. A cubic spline implementation of nonlinear shear behaviour in three-dimensional progressive damage models for composite laminates. *Composite Structures*, 92(1):173–181, 2010.
30. E.K Gamstedt and Sjögren. Micromechanisms in tension-compression fatigue of composite laminates containing transverse plies. *Composites Science and Technology*, 59(2):167–178, 1999.
31. E. Pineda, B. Bednarcyk, A. M. Waas, and S. Arnold. Progressive Failure of a Unidirectional Fiber-reinforced Composite Using the Method of Cells: Discretization Objective Computational Results. *53rd AIAA/ASME/ASCE/AHS/ASC Structures, Structural Dynamics and Materials Conference 20th AIAA/ASME/AHS Adaptive Structures Conference*, (April):1–46, 2012.